SCIENCE CHINA
Information Sciences

• MOOP •

October 2023, Vol. 66 204101:1–204101:3
https://doi.org/10.1007/s11432-023-3779-5

A unified user behavior model for trajectory-based tasks with different types of path constraints

Hao ZHANG[1,2], Jin HUANG[1,3*], Huawei TU[4], Feng TIAN[1,3], Guozhong DAI[1] & Hongan WANG[1]

[1]*Beijing Key Laboratory of Human-Computer Interaction, Institute of Software Chinese Academy of Sciences, Beijing* 100190*, China;*
[2]*School of Computer Science and Technology, University of Chinese Academy of Sciences, Beijing* 101408*, China;*
[3]*School of Artificial Intelligence, University of Chinese Academy of Sciences, Beijing* 101408*, China;*
[4]*Department of Computer Science and Information Technology, La Trobe University, Melbourne* VIC 3086*, Australia*

Received 10 January 2023/Accepted 21 March 2023/Published online 27 September 2023

Citation Zhang H, Huang J, Tu H W, et al. A unified user behavior model for trajectory-based tasks with different types of path constraints. Sci China Inf Sci, 2023, 66(10): 204101, https://doi.org/10.1007/s11432-023-3779-5

An important research branch of human-computer interaction (HCI) is to develop predictive models for human performance in fundamental interactions [1]. On today's graphical user interface (GUI), users often implicitly perform various trajectory-based interactions, such as navigating through menus [2], entering the boundary of a button, and lassoing regularly arranged icons [3]. These interactions allow users to select targets or input commands in user interfaces by drawing strokes. Based on these fundamental interactions on GUI, researchers explored three typical trajectory-based tasks with different path constraints: the steering task [4], the goal-crossing task [4], and the steering-crossing task [5]. For trajectory-based tasks, the movement profile information encompassing trajectory, speed, and cursor acceleration emerges as a valuable tool for characterizing user performance. Such information could be crucial in understanding user behaviors in user interfaces. However, existing models tend to fixate on the prediction of interaction outcomes such as movement time or error rates. This prevailing focus creates a theoretical gap, resulting in a challenge for HCI practitioners to gain a comprehensive grasp of the intricate and dynamic nature of user engagement during trajectory-based interactions.

In general, no matter what path constraints a trajectory-based task has, the user always needs to navigate an interactive device (e.g., a stylus) to achieve a goal while avoiding obstacles along the way. Dynamic models like artificial potential field (APF) [6] or feedback control models like optimal feedback control (OFC) [1] can be used to solve such modeling problems. Notably, APF presents a distinct advantage over OFC in its ability to adapt to environmental dynamics without incessant recalibration. Within the framework of APF, the environment is divided into two types of potentials: attractive potential and repulsive potential. Each of these potentials creates a scalar field that assigns a value to every point in the environment. The value of the scalar field at a particular point represents the "strength" of the potential at that point. The agent calculates the gradient of the combined potential field at its present position to determine its course of action. This results in a natural tendency for the agent to move toward the target while avoiding obstacles. This behavior closely mimics the way that humans behave in trajectory-based tasks.

However, constructing an APF-based model that simulates user performance in HCI tasks has the following challenges. First, given the diversity of HCI tasks, the model should be robust enough to be applied to different tasks. Second, the original APF cannot simulate human behavior uncertainty in performing HCI tasks (e.g., uncertainty in movement, speed, or decision making). Finally, the cursor speed should be controlled within the range of human joint motion capabilities.

To address the above issues, we formulated different types of trajectory-based tasks to a unified description based on APF and established a computational model that can simulate user movements.

Basic concepts. We first introduce fundamental concepts of our model: Task Space denotes the area in which the task is performed by the user. Particle represents the user-controlled cursor. The Goal represents the destination that the cursor is directed toward. Our model includes two goal types: Final Goal and Temporary Goal. Final Goal is the final target area of the trajectory-based tasks. Temporary Goal is a local destination within the cursor's Visual Field. Obstacle defines task boundaries. Visual Field, a fan-shaped region centered around the cursor, generates Temporary Goals based on local boundaries to guide cursor movements.

Attractive Potential and Forces. The Attractive Potential generates a force driving the Particle toward its center. The center of the Attractive Potential aligns with the center

* Corresponding author (email: huangjin@iscas.ac.cn)

of the Goal. The force's derivation involves calculating the gradient of the Attractive Potential $U_{att}(t)$, resulting in the Attractive Force $F_{att}(t)$, given by:

$$F_{att}(t) = -\nabla U_{att}(t) = -\frac{1}{2} - \nabla \rho_{goal}^2(p) = -k\rho_{goal}(p), \quad (1)$$

where $\rho_{goal}(p) = \left\| p - p_{goal} \right\|$ represents the Euclidean distance between the Particle and the center of the Attractive Potential, and k is a positive scaling factor.

Repulsive Potential and Forces. The center of the Repulsive Potential is usually located at a specific point on the Obstacle, determined by the relative spatial relationship between the Particle and the Obstacle. To mitigate the local potential field minima issue, we adopt a modified Repulsive Potential [7]. The repulsive force $F_{rep}(t)$ derived from the Repulsive Potential $U_{rep}(t)$ is calculated as:

$$\begin{aligned} &F_{rep}(t) = \nabla U_{rep}(t) \\ &= \begin{cases} 0, & \rho(p) > \rho_0, \\ \|F_{repp}(t)\| \, \boldsymbol{n_p} + \|F_{repg}(t)\| \, \boldsymbol{n_{goal}}, & \rho(p) \leqslant \rho_0. \end{cases} \end{aligned} \quad (2)$$

The Repulsive Potential generates forces in two directions: one from the Particle to the center of the Repulsive Potential $\boldsymbol{n_p}$, and the other from the Particle to the Final Goal $\boldsymbol{n_{goal}}$. Within these directions, $F_{rep}(t)$ splits into sub-forces: $F_{repp}(t)$ and $F_{repg}(t)$, calculated as:

$$\|F_{repp}(t)\| = \eta \left(\frac{1}{\rho(p)} - \frac{1}{\rho_0} \right) \frac{\rho_{goal}^2(p)}{\rho^2(p)}, \quad (3)$$

$$\|F_{repg}(t)\| = \eta \left(\frac{1}{\rho(p)} - \frac{1}{\rho_0} \right)^2 \rho(p), \quad (4)$$

where η is a positive constant, $\rho(p) = \|p - p(p)\|$ denotes the minimal distance from the Particle to the center of the Repulsive Potential, and ρ_0 is a positive constant denoting the influence range of the Repulsive Potential.

Modified artificial potential field model. In our model, the state $X(t)$ of the Particle at time t can be expressed as:

$$X(t) = [F(t), v(t), x(t), y(t)], \quad (5)$$

where $F(t)$ is the combined force of the Particles. It consists of two parts; one is the force F_U generated by the total potential $U(t)$, the other is the perturbing force F_{per} perpendicular to the moving direction of the Particle. $v(t)$ is the Particle's speed and can be calculated by the combined force $F(t)$ using Newton's second law. $(x(t), y(t))$ is the position of the Particle.

(1) Given an initial status (e.g., still at the starting area), our approach initially transforms the Task Space into computable potentials. The total potential $U(t)$ comprises four constituent components:

• Repulsive Potential U_{Orep}. This component aggregates the Repulsive Potentials enveloping the Particle within the Task Space. It detects Obstacles across multiple directions and aligns its center at the intersections of extended lines and the Obstacle's edges, thus guaranteeing obstacle avoidance.

• Attractive Potential U_{Tatt}. Centered around the Temporary Goal, it generates an attractive force guiding the Particle towards the Temporary Goal.

• Repulsive Potential U_{Grep}. Positioned around the Final Goal, it typically consists of two Repulsive Potentials, each centered at an end of the bar-shaped goal. These potentials yield forces that guide the Particle toward the Final Goal's center.

• Attractive Potential U_{Gatt}. Positioned at the center of the Final Goal, this component generates an Attractive Force that propels the Particle toward the final target area.

To compute the total potential, we sum the attractive and repulsive potentials, subsequently deriving the force $F_U(t)$ through partial differentiation:

$$\begin{aligned} F_U(t) &= -\nabla U(t) = \nabla U_{Orep} + \nabla U_{Grep} \\ &- \nabla U_{Tatt} - \left(1 - \frac{\rho_{G-goal}(p)}{\rho_{G-goal}(p_0)} \right) \nabla U_{Gatt}, \end{aligned} \quad (6)$$

where $\rho_{G-goal}(p_0)$ is the distance between the Particle's initial position and the Final Goal, $\rho_{G-goal}(p)$ is the distance between its current position and the Final Goal. All the potentials and their corresponding forces in (6) are computed following the principles outlined in (1)–(4).

(2) We introduce a perturbing force $F_{per}(t)$ to account for hand movement uncertainties. This force acts perpendicular to the hand's movement direction and follows a Gaussian distribution $N_{per} \sim N(0, \sigma)$. The standard deviation(σ) of the perturbing force is linearly related to the Particle's current speed $v(t)$, expressed as:

$$\sigma = av(t) + b, \quad (7)$$

where a and b are constants. By adding this uncertainty adjustment to (6), the final combined force $F(t)$ acting on the Particle is obtained:

$$F(t) = F_U(t) + F_{per}(t) = F_U(t) + N_{per}\boldsymbol{n_v}, \quad (8)$$

where the vector $\boldsymbol{n_v}$ denotes the current movement's normal direction. The cumulative impact of these forces ultimately dictates the precise movement of the Particle.

(3) Movement status update. Differing from simple physical simulations without restrictions, human movement simulations need to account for inherent behavioral patterns. We developed a preferred speed model to govern the Particle's maximum velocity based on the tunnel width. The preferred speed V_{pref} of the Particle is determined as

$$V_{pref} = cW + d, \quad (9)$$

where c and d are constants and W is the width of the tunnel. According to Newton's second law, (8), and (9), the Particle's speed at next frame $v(t+1)$ can be calculated as:

$$v(t+1) = \min \left(v(t) + \frac{F(t)}{m} \triangle t, V_{pref} \right), \quad (10)$$

where $F(t)$ is the combined force calculated by (8), $v(t)$ is the speed at time t, and $\triangle t$ is the time difference between two frames. Finally, the Particle's position in the next frame $p_{t+1} = (x_{t+1}, y_{t+1})$ can be calculated as

$$p_{t+1} = p_t + v(t+1) \triangle t, \quad (11)$$

where $p_t = (x(t), y(t))$ denotes the Particle's current position at current time t, and $v(t+1)$ is the Particle's speed derived from (10). This incremental update process continues until the Particle reaches the target area. Further details are available in Appendix A.

Model evaluation. As shown in Figures 1(a)–(d), we evaluated our model in three conventional trajectory-based tasks (i.e., steering, goal-crossing, and steering-crossing tasks) and a newly introduced randomized setting called randomized

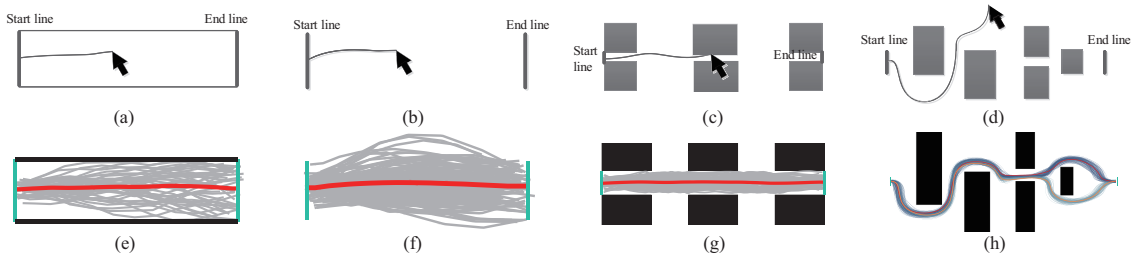

Figure 1 (a–d) Various trajectory-based tasks: steering task, goal-crossing task, steering-crossing task with regular obstacle intervals, and randomized steering task. (e–h) Simulated cases for each of these tasks.

steering task. The results consistently demonstrated that our model fits the data in terms of the mean trajectory, movement uncertainty, and movement time in these tasks.

Concerning the movement time, the mean absolute error (MAE) values of the first three conventional tasks are 36.77, 17.20, and 86.59 ms. For the randomized steering task, the MAE is 259.63 ms. These MAE values correspond to 6.92%, 5.65%, 4.42%, and 9.26% of the total movement time, respectively. Regarding the mean trajectory, the MAEs for the four tasks are 5.59, 10.16, 20.28, and 41.16 *mm*, respectively. These MAE values represent 4.93%, 9.60%, 7.64%, and 10.44% of the overall length of the mean trajectory. As for the movement uncertainty, the MAEs of movement variability between actual and simulated trajectories for the four tasks are 0.62, 3.52, 0.57, and 17.70 mm, respectively. Simulated cases of each task are illustrated in Figures 1(e)–(h). For a detailed evaluation, please refer to Appendixes B and C.

Relationship between path constraints and movement uncertainty. We found a notable performance difference between the steering and goal-crossing tasks, despite their identical goal width (W) and length (A). Users exhibited distinct behaviors: the average movement time was 509.96 ms for the steering task and 340.11 ms for the goal-crossing task. The goal-crossing task appeared simpler for users but resulted in higher trajectory uncertainty: 6.95 mm of movement variability for goal-crossing versus 1.40 mm for steering. This indicates that lower path constraints could lead to greater movement uncertainty.

Uncertainty of decision-making. In the randomized steering task, when the Particle encountered the last wall-like obstacle, the route forked into two paths due to the obstacle. Human behavior demonstrated that individuals don't consistently choose the same route at such junctures (Figure 1(h)). Our model simulates this decision-making uncertainty in trajectory-based tasks. Specifically, at the fork, the perturbing force introduced random lateral disturbance, slightly shifting the cursor's movement direction (upward or downward). This shift influenced the selection of the Temporary Goal within the Particle's Visual Field, which aligns with the motion direction. The chosen Temporary Goal was then amplified by the attractive force, leading to a greater turn. This dual approach effectively mimics the trajectory uncertainty arising from user decision-making.

Future work. Our study did not explore trajectory-based gestures (e.g., swiping and pinching) that lack trajectory path constraints. Such tasks could exhibit significant trajectory uncertainty due to the absence of constraints. In these gesturing tasks, the cognitive complexity involved in perceiving and planning gestures might significantly influence user performance. Modeling these gestures using our approach might necessitate initial modeling of the user's cognitive gesture-drawing process. This avenue will be a focus of our future research.

Conclusion. We introduced a novel approach that combines the speed-accuracy trade-off theory with APF to characterize user behaviors in HCI. Our model's validation across four distinct trajectory-based tasks showcased its adeptness at fitting experimental data, encompassing the movement time, mean trajectory, and movement uncertainty. Moreover, our model's simulated trajectories can supply designers with valuable user performance insights even when participant numbers are limited.

Acknowledgements This work was supported by National Natural Science Foundation of China (Grant Nos. 62132010, 62172397), CAS Project for Young Scientists in Basic Research (Grant No. YSBR-040), and Youth Innovation Promotion Association CAS (Grant No. 2020113).

Supporting information Appendixes A–C, videos, and other supplemental documents. The supporting information is available online at info.scichina.com and link.springer.com. The supporting materials are published as submitted, without typesetting or editing. The responsibility for scientific accuracy and content remains entirely with the authors.

References

1 Huang J, Peng X L, Tian F, et al. Modeling a target-selection motion by leveraging an optimal feedback control mechanism. Sci China Inf Sci, 2018, 61: 044101
2 Lyu F, Liu Y J, Huang J, et al. LotusMenu: a 3D menu using wrist and elbow rotation inspired by Chinese traditional symbol. Sci China Inf Sci, 2021, 64: 204101
3 Henke K, Teti M, Kenyon G, et al. Apples-to-spikes: the first detailed comparison of LASSO solutions generated by a spiking neuromorphic processor. In: Proceedings of the International Conference on Neuromorphic Systems, 2022. 1–8
4 Accot J, Zhai S. Beyond Fitts' law: models for trajectory-based HCI tasks. In: Proceedings of Extended Abstracts on Human Factors in Computing Systems, 1997. 295–302
5 Yamanaka S, Stuerzlinger W, Miyashita H. Steering through successive objects. In: Proceedings of the CHI Conference on Human Factors in Computing Systems, 2018. 1–13
6 Das M S, Sanyal S, Mandal S. Navigation of multiple robots in formative manner in an unknown environment using artificial potential field based path planning algorithm. Ain Shams Eng J, 2022, 13: 101675
7 Liu J, Li C S. A new method to solve the local minimum problem of an artificial potential field (in Chinese). In: Proceedings of the 15th China Mechanical Design Convention, 2009. 76–78, 85